

Edge multiscale finite element methods for semilinear parabolic problems with heterogeneous coefficients

Leonardo A. Poveda* Shubin Fu† Guanglian Li‡ Eric T. Chung§

October 29, 2024

Abstract

We develop a new spatial semidiscrete multiscale method based upon the edge multiscale methods to solve semilinear parabolic problems with heterogeneous coefficients and smooth initial data. This method allows for a cheap spatial discretization, which fails to resolve the spatial heterogeneity but maintains satisfactory accuracy independent of the heterogeneity. This is achieved by simultaneously constructing a steady-state multiscale ansatz space with certain approximation properties for the evolving solution and the initial data. The approximation properties of the multiscale ansatz space are derived using local-global splitting. A fully discrete scheme is analyzed using a first-order explicit exponential Euler scheme. We derive the error estimates in the L^2 -norm and energy norm under the regularity assumptions for the semilinear term. The convergence rates depend on the coarse grid size and the level parameter. Finally, extensive numerical experiments are carried out to validate the efficiency of the proposed method.

1 Introduction

We consider in this paper the efficient multiscale method for a semilinear parabolic equation with heterogeneous coefficient κ in the form

$$\partial_t u - \nabla \cdot (\kappa \nabla u) + \beta \cdot \nabla u = R(x, u)$$

*Department of Mathematics, The Chinese University of Hong Kong, Hong Kong (lpoveda@math.cuhk.edu.hk)

†Eastern Institute for Advanced Study, Eastern Institute of Technology, Ningbo, Zhejiang 315200, P. R. China (sfu@eitech.edu.cn)

‡Department of Mathematics, University of Hong Kong, Pokfulam, Hong Kong (lotusli@maths.hku.hk). GL acknowledges the support from GRF (project number: 17317122) and Early Career Scheme (Project number: 27301921), RGC, Hong Kong.

§Department of Mathematics, The Chinese University of Hong Kong, Hong Kong (eric.t.chung@cuhk.edu.hk)

with certain boundary conditions and initial conditions. Here, $R(x, u)$ denotes the reaction term that can be nonlinear. This model type occurs in many applications, such as the phase field problems in the Allen-Cahn equation, which describes phase transition and separation (Allen and Cahn, 1979). Other examples include the Ginzburg-Landau equation that studies the behavior of superconductivity (Caliari and Cassini, 2024), the Navier-Stokes equations in highly heterogeneous media, which are used for the study of fluid dynamics and multiphase problems (Muljadi et al., 2015).

Classical numerical methods, such as finite element methods, resolve the coefficient's heterogeneity to obtain a solution with sufficient accuracy, resulting in huge computational complexity. During the last few decades, many multiscale model reduction techniques have been developed and analyzed to make computational complexity independent of the multiple scales, such as multiscale finite element methods (Hou and Wu, 1997), multiscale variational methods (Hughes et al., 1998), heterogeneous multiscale methods (E and Engquist, 2003), multiscale mortar methods (Arbogast et al., 2007), localized orthogonal decomposition methods (Målqvist and Peterseim, 2014), generalized multiscale finite element methods (Efendiev et al., 2013; Chung et al., 2023). These methods have demonstrated extremely satisfactory numerical results for various problems and have become increasingly popular. In this work, we will consider the Edge Multiscale Methods (EMsFEM), which was initially proposed in Li (2019); Fu et al. (2019) and has been applied to several linear problems with heterogeneous coefficients Fu et al. (2021); Li and Hu (2021); Fu et al. (2023); Li (2024). Its main idea is to first construct a local splitting of the solution on a sequence of overlapping subdomains, and then establish the global splitting by means of the partition of unity functions Melenk and Babuška (1996). In this manner, the global error estimate is determined by the local error estimate in each subdomain. Consequently, deriving the local error estimate is the crucial task in the analysis. Its proof is inspired by the transposition method that provides *a priori* estimate in weighted L^2 -norm of the homogeneous elliptic problem with nonhomogeneous Dirichlet boundary data in weighted L^2 -norm Lions and Magenes (1972). The semilinearity makes the local splitting nontrivial, and the multiscale basis functions potentially rely on the nonlinear term. However, upon assuming the boundedness of the first-order partial derivative of the nonlinear term with respect to the solution, we prove that the multiscale space is independent of the semilinear term, and thus, one multiscale space is sufficient for all time steps. The local error estimate is presented in Lemma 3.3. Based upon this, we can derive an error estimate for the elliptic projection in Lemma 3.4, then a standard error estimate yields the semidiscrete error estimate in Theorem 3.5.

Moreover, standard numerical approaches such as implicit methods have been proposed and analyzed for temporal discretization, which are attractive due to their unconditional stability. However, they involve solving nonlinear equations at each time step and thus are computationally expensive. In contrast, Exponential integrators are robust, with the linear part handled exactly and the non-linear part explicitly (Hochbruck and Ostermann, 2010; Caliari et al., 2024; Contreras et al., 2023; Poveda et al., 2024), and we explore their

performance for this semilinear parabolic problem. We present a rigorous convergence analysis of the proposed method under smooth initial data and certain regularity of the semilinear term in Theorem 4.2, validated by extensive numerical experiments.

The outline of the paper is as follows. Section 2 is dedicated to the problem of the model and its spatial discretization. The multiscale edge space is constructed in Section 3. Section 3.3 presents the construction of the hierarchical bases. In Section 4, we present the explicit exponential method. Under appropriate assumptions of the exact solution and the nonlinear reaction term, we show the fully discrete error analysis of the proposed approach. Numerical experiments are provided in Section 5. Finally, conclusions and final comments are drawn in Section 6.

2 Problem setting

We are concerned with the semilinear parabolic problem

$$\begin{aligned} \partial_t u - \nabla \cdot (\kappa \nabla u) + \boldsymbol{\beta} \cdot \nabla u &= R(\cdot, u) & \text{in } D \times (0, T] \\ u(\cdot, 0) &= u_0 & \text{in } D \\ u(\cdot, t) &= 0 & \text{on } \partial D \times (0, T]. \end{aligned} \tag{2.1}$$

Let D be a domain with $C^{1,\alpha}$, ($0 < \alpha < 1$) boundary ∂D , and $\{D_i\}_{i=1}^m \subset D$ be M pairwise disjoint strictly convex open subsets, each with a $C^{1,\alpha}$ boundary $\Gamma_i := \partial D_i$, and denote $D_0 = D \setminus \overline{\bigcup_{i=1}^m D_i}$. Let the permeability coefficient κ be a piecewise regular function defined by

$$\kappa(\mathbf{x}) = \begin{cases} \eta_i(\mathbf{x}), & \text{in } D_i, \\ 1, & \text{in } D_0. \end{cases}$$

Here, $\eta_i \in C^{0,\nu}(\overline{D_i})$ with $\nu \in (0, 1)$ for $i = 1, \dots, m$. We denote $\eta_{\min} := \min_i \{\|\eta_i\|_{C^0(D_i)}\} \geq 1$ and $\eta_{\max} := \max_i \{\|\eta_i\|_{C^0(D_i)}\}$. We further assume that $\eta_{\min} \gg 1$, and η_{\min} has the same magnitude as η_{\max} . $\boldsymbol{\beta} \in [L^\infty(D)]^d$ represents the advective vector field, which is incompressible, *i.e.*, $\nabla \cdot \boldsymbol{\beta} = 0$. $R(\mathbf{x}, u)$ is often interpreted as a reaction term (possibly non-linear), assuming smooth on $D \times \mathbb{R}$, and $R(\mathbf{x}, \cdot)$ is uniformly Lipschitz continuous on D .

We assume the initial data $u_0 \in \dot{H}^2(D)$, with

$$\dot{H}^2(D) := \{v \in V := H_0^1(D) : \mathcal{L}v := -\nabla \cdot (\kappa \nabla v) + \boldsymbol{\beta} \cdot \nabla v \in L^2(D)\}.$$

Throughout this paper, $x \preceq y$ means a positive constant C exists independent of κ and mesh size h to be introduced, such that $x \leq Cy$, and $x \simeq y$ means $y \preceq x \preceq y$. Furthermore, we introduce the following assumptions related to the growth condition for the reaction term R and the regularity estimates for solution u , see Thomée (2006).

Assumption 2.1. *The function $R(\mathbf{x}, v)$ grows mildly with respect to v , i.e., there exists a number $p > 0$ for $d = 2$ or $p \in (0, 2]$ for $d = 3$ such that,*

$$\left| \frac{\partial R}{\partial v}(\mathbf{x}, v) \right| \preceq 1 + |v|^p, \quad \text{for each } v \in \mathbb{R} \text{ and } \mathbf{x} \in D. \quad (2.2)$$

Moreover, $R(\mathbf{x}, 0) = 0$ for all $\mathbf{x} \in D$.

Lemma 2.2. *Let $u_0 \in \dot{H}^2(D)$, and let Assumption 2.1 hold. Then Problem (2.1) is well-posed, and its solution $u(\cdot, t)$ has the following regularity properties,*

$$\|\mathcal{L}u(\cdot, t)\|_{L^2(D)} \preceq 1, \quad \text{for } t \in [0, T], \quad (2.3a)$$

$$\|\partial_t u(\cdot, t)\|_{L^2(D)} \preceq 1, \quad \text{for } t \in [0, T], \quad (2.3b)$$

$$\|\mathcal{L}^{1/2} \partial_t u(\cdot, t)\|_{L^2(D)} \preceq t^{-1/2}, \quad \text{for } t \in (0, T]. \quad (2.3c)$$

Lemma 2.3 (Larsson, 1992, Lemma 2.1). *Suppose the function R satisfies Assumption 2.1. Then for any $v, w \in V$, there holds*

$$\|R(\cdot, v) - R(\cdot, w)\|_{H^{-1}(D)} \preceq \|v - w\|_{L^2(D)}, \quad (2.4a)$$

$$\|R(\cdot, v) - R(\cdot, w)\|_{L^2(D)} \preceq \|v - w\|_{H^1(D)}. \quad (2.4b)$$

Next, we introduce the weak formulation of (2.1), which reads as seeking $u(\cdot, t) \in V$ such that

$$\begin{aligned} (\partial_t u, v) + A(u, v) &= (R(\cdot, u), v), \quad \text{for all } v \in V, \\ u(\cdot, 0) &= u_0, \end{aligned} \quad (2.5)$$

with (\cdot, \cdot) denoting the inner product in $L^2(D)$, $A(u, v) := a(u, v) + (\boldsymbol{\beta} \cdot \nabla u, v)$, and

$$a(u, v) := \int_D \kappa \nabla u \cdot \nabla v \, dx.$$

Since that $\nabla \cdot \boldsymbol{\beta} = 0$, the bilinear form $A(\cdot, \cdot)$ in (2.5) is V-elliptic, i.e.,

$$A(v, v) = \|\nabla v\|_{L^2_\kappa(D)}^2, \quad \text{for each } v \in V. \quad (2.6)$$

Here, $\|\nabla v\|_{L^2_\kappa(D)}^2 := a(v, v)$.

An application of the Friedrichs' inequality implies the boundedness of the bilinear form $A(\cdot, \cdot)$,

$$|A(u, v)| \leq C \|\nabla u\|_{L^2_\kappa(D)} \|\nabla v\|_{L^2_\kappa(D)},$$

where the positive constant C depends on diameter of the domain D and $\|\boldsymbol{\beta}\|_{L^\infty(D)}$.

3 The edge multiscale method

We present in this section the edge multiscale method to solve (2.1) for $d = 2$ only for simplicity. The generalization of this method to $d = 3$ can be followed similarly. The main idea of this approach is that first, we generate a coarse mesh \mathcal{T}_H on the spatial domain D , which cannot resolve the microscale feature in the coefficient κ and then introduce a sequence of overlapping subdomains using \mathcal{T}_H . Note that standard numerical methods cannot produce a reasonable solution under this coarse mesh \mathcal{T}_H due to the pre-asymptotic effect. Second, we derive a local splitting of the solution on each subdomain by a summation of a local bubble function and a local Harmonic extension function. In contrast, the former can be solved locally, and the latter can be defined over the internal edges of the coarse mesh \mathcal{F}_H . This local splitting induces naturally a global splitting using the partition of unity functions. Third, we propose to use hierarchical bases up to level ℓ as the ansatz space for the solution on \mathcal{F}_H . The most crucial component in the theoretical analysis is to transfer the approximation properties over the coarse skeleton \mathcal{F}_H to the internal of each subdomain without extra regularity assumptions on the solution. This was first proved in (Li, 2019, Appendix A) by defining a very weak solution in each subdomain and establishing an *a priori* estimate inspired by the transposition method in Lions and Magenes (1972).

3.1 Discretization

First, we introduce a cheap discretization of the computational domain D that fails to resolve the multiple scales in the heterogeneous coefficient κ . Let \mathcal{T}_H be a regular partition of the domain D into quasi-uniform quadrilaterals with mesh size H . Let $\mathcal{F}_H := \cup_{T \in \mathcal{T}_H} \partial T \setminus \partial D$ be the collection of internal edges in \mathcal{T}_H . The set of nodes of \mathcal{T}_H are denoted by $\{\mathbf{x}_i\}_{i=1}^N$, with N being the total number of coarse nodes. The coarse neighborhood associated with the node \mathbf{x}_i is denoted by

$$\omega_i := \overline{\bigcup \{K_j \in \mathcal{T}_H : \mathbf{x}_i \in \overline{K_j}\}}.$$

We defined the overlapping constant C_{ov} by

$$C_{\text{ov}} := \max_{K \in \mathcal{T}_H} \#\{\mathbf{x}_i : K \in \omega_i, \text{ for } i = 1, \dots, N\}. \quad (3.1)$$

Next, we introduce the partition of unity $\{\chi_i\}_{i=1}^N$ subordinate to the sequence of overlapping subdomains $\{\omega_i\}_{i=1}^N$ that satisfies

$$\text{supp}(\chi_i) \subset \bar{\omega}_i, \quad \sum_{i=1}^N \chi_i = 1 \text{ in } D, \quad \|\chi_i\|_{L^\infty(\omega_i)} \leq C_\infty, \quad \|\nabla \chi_i\|_{L^\infty(\omega_i)} \leq C_G H^{-1}$$

with C_∞ and C_G being positive constants independent of κ , h and H .

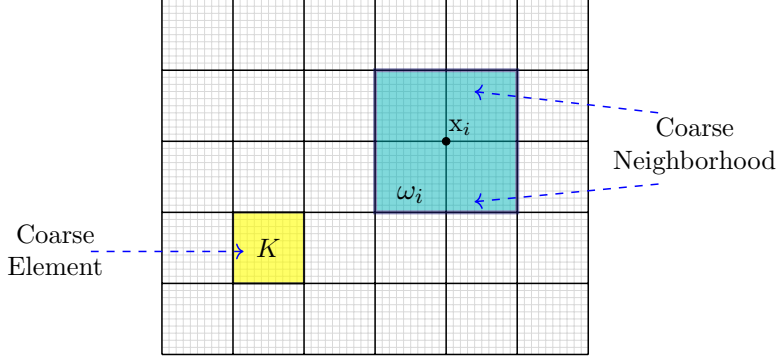


Figure 1: 2-d coarse grid \mathcal{T}_H , where K and ω_i denote a coarse element and the coarse neighborhood associated with the node x_i .

Then, we define the weighted coefficient:

$$\tilde{\kappa} = H^2 \kappa \sum_{i=1}^N |\nabla \chi_i|^2, \quad (3.2)$$

and the weighted $L^2(D)$ space

$$L_{\tilde{\kappa}}^2(D) := \left\{ w : \|w\|_{L_{\tilde{\kappa}}^2(D)}^2 := \int_D \tilde{\kappa} w^2 dx < \infty \right\}.$$

3.2 Local-global splitting

Note that the solution u of problem (2.1) satisfies

$$\mathcal{L}_i u := \nabla \cdot (\kappa \nabla u) + \beta \cdot \nabla u = R(\cdot, u) - \partial_t u, \quad \text{in } \omega_i,$$

which can be split into the summation of two parts,

$$u|_{\omega_i} = u^{i,\text{I}} + u^{i,\text{II}}. \quad (3.3)$$

Here, each component $u^{i,\text{I}}$ and $u^{i,\text{II}}$ are given by

$$\begin{cases} \mathcal{L}_i u^{i,\text{I}} = R(\cdot, u) - \partial_t u, & \text{in } \omega_i, \\ u^{i,\text{I}} = 0, & \text{on } \partial \omega_i, \end{cases} \quad (3.4)$$

and

$$\begin{cases} \mathcal{L}_i u^{i,\text{II}} = 0, & \text{in } \omega_i, \\ u^{i,\text{II}} = u, & \text{on } \partial \omega_i \setminus \partial D \\ u^{i,\text{II}} = 0, & \text{on } \partial \omega_i \cap \partial D. \end{cases} \quad (3.5)$$

Observe that $u^{i,\text{I}}$ contains the local information that can be solved locally, and $u^{i,\text{II}}$ encodes the global information over the inner coarse skeleton \mathcal{F}_H . This local splitting induces a global splitting of u by means of the partition of unity functions,

$$u = \left(\sum_{i=1}^N \chi_i \right) u = \sum_{i=1}^N \chi_i u|_{\omega_i} = \sum_{i=1}^N \chi_i (u^{i,\text{I}} + u^{i,\text{II}}) := u^{\text{I}} + u^{\text{II}}, \quad (3.6)$$

where

$$u^{\text{I}} = \sum_{i=1}^N \chi_i u^{i,\text{I}} \text{ and } u^{\text{II}} = \sum_{i=1}^N \chi_i u^{i,\text{II}}. \quad (3.7)$$

3.3 Hierarchical bases

Next, we introduce the hierarchical bases on the unit interval $I := [0, 1]$, which facilitates hierarchically splitting the space $L^2(I)$.

Let the level parameter and the mesh size be ℓ and $h_\ell =: 2^{-\ell}$ with $\ell \in \mathbb{N}$. Then, the grid points on level ℓ are

$$x_{\ell,j} = j \times h_\ell, \quad 0 \leq j \leq 2^\ell.$$

We can define the basis functions on level ℓ by

$$\psi_{\ell,j}(x) : \begin{cases} 1 - \left| \frac{x}{h_\ell - j} \right|, & \text{if } x \in [(j-1)h_\ell, (j+1)h_\ell] \cap [0, 1], \\ 0, & \text{otherwise.} \end{cases}$$

Define the set on each level ℓ by

$$B_\ell := \left\{ j \in \mathbb{N} : \begin{cases} j = 1, \dots, 2^\ell - 1, j \text{ is odd}, & \text{if } \ell > 0 \\ j = 0, 1, & \text{if } \ell = 0 \end{cases} \right\}.$$

The subspace of level ℓ is

$$W_\ell := \text{span}\{\psi_{\ell,j} : j \in B_\ell\}.$$

We denote V_ℓ as the subspace in $L^2(I)$ up to level ℓ , which is defined by the direct sum of subspaces

$$V_\ell := \bigoplus_{m \leq \ell} W_m.$$

Consequently, this yields the hierarchical structure of the subspace V_ℓ , namely

$$V_0 \subset V_1 \subset \dots \subset V_\ell \subset V_{\ell+1} \dots$$

Furthermore, the following hierarchical decomposition of the space $L^2(I)$ holds

$$L^2(I) = \lim_{\ell \rightarrow \infty} \bigoplus_{m \leq \ell} W_m.$$

Note that one can derive the hierarchical decomposition of the space $L^2(I^{d-1})$ for $d > 1$ through the tensor product, which is denoted as $V_\ell^{\otimes d-1}$. We will use the subspace V_ℓ to approximate the exact solution u restricted on \mathcal{F}_H .

Next, we present the approximation properties of the hierarchical space V_ℓ , which can be derived from standard L^2 -projection error [Ciarlet \(1978\)](#) combining with the interpolation method.

Proposition 3.1 (Approximation properties of the hierarchical space V_ℓ). *Let $d = 2, 3$, $s > 0$ and let $\mathcal{I}_\ell : L^2(I^{d-1}) \rightarrow V_\ell^{\otimes d-1}$ be L^2 -projection for each level $\ell \geq 0$, then there holds,*

$$\|v - \mathcal{I}_\ell v\|_{L^2(I^{d-1})} \lesssim 2^{-s\ell} |v|_{H^s(I^{d-1})} \quad \text{for all } v \in H^s(I^{d-1}). \quad (3.8)$$

Here, $|\cdot|_{H^s(I^{d-1})}$ denotes the Gagliardo seminorm in the fractional Sobolev space (or Slobodetskii space) $H^s(I^{d-1})$, given by

$$|v|_{H^s(I^{d-1})}^2 := \int_{I^{d-1}} \int_{I^{d-1}} \frac{|v(x) - v(y)|^2}{|x - y|^{d-1+2s}} dx dy.$$

The corresponding full norm is denoted as $\|\cdot\|_{H^s(I^{d-1})}$.

3.4 Edge multiscale ansatz space

Next, we introduce the construction of the edge multiscale ansatz space.

First, we define the linear space over the inner boundary of each coarse neighborhood $\partial\omega_i \setminus \partial D$. Let the level parameter $\ell \in \mathbb{N}$ be fixed, and let Γ_i^k with $k = 1, 2, 3, 4$ be a partition of $\partial\omega_i \setminus \partial D$ with no mutual intersection, *i.e.*, $\cup_{k=1}^4 \overline{\Gamma_i^k} = \partial\omega_i \setminus \partial D$ and $\Gamma_i^k \cap \Gamma_i^{k'} = \emptyset$ if $k \neq k'$. Furthermore, we denote $E_{i,\ell}^k \subset C(\partial\omega_i)$ as the linear space spanned by hierarchical bases up to level ℓ on each coarse edge Γ_i^k and continuous over $\partial\omega_i$, then the local edge space $E_{i,\ell}$ defined over $\partial\omega_i$ is the smallest linear space having $E_{i,\ell}^k$ as a subspace. Let $\{\psi_{i,\ell}^j\}_{j=1}^{2^{\ell+2}}$ and $\{x_{i,\ell}^j\}_{j=1}^{2^{\ell+2}}$ be the nodal basis functions and the associated nodal points for $E_{i,\ell}$, then we can represent the local edge space $E_{i,\ell}$ by

$$E_{i,\ell} := \text{span} \left\{ \psi_{i,\ell}^j : 1 \leq j \leq 2^{\ell+2} \right\}. \quad (3.9)$$

Next, we introduce the local multiscale space over each coarse neighborhood ω_i , which is defined by

$$\mathcal{L}_i^{-1}(E_{i,\ell}) := \text{span} \left\{ \mathcal{L}_i^{-1}(\psi_{i,\ell}^j) : 1 \leq j \leq 2^{\ell+2} \right\}. \quad (3.10)$$

Here, $\mathcal{L}_i^{-1}(\psi_{i,\ell}^j) := v \in H^1(\omega_i)$ is the solution to the following local problem,

$$\begin{cases} \mathcal{L}_i v := -\nabla \cdot (\kappa \nabla v) + \beta \cdot \nabla v = 0 & \text{in } \omega_i, \\ v = \psi_{i,\ell}^j & \text{on } \partial\omega_i \setminus \partial D \\ v = 0 & \text{on } \partial\omega_i \cap \partial D. \end{cases} \quad (3.11)$$

By this construction, the dimension of $\mathcal{L}_i^{-1}(E_{i,\ell})$ equals $2^{\ell+2}$. In practice, a number of $2^{\ell+2}$ local problems (3.11) are solved by the standard numerical methods such as the FEMs with sufficient accuracy to obtain the local multiscale space $\mathcal{L}_i^{-1}(E_{i,\ell})$, which can be solved in parallel and thus has low computational complexity.

Finally, the edge multiscale ansatz space is defined by the Partition of Unity $\{\chi_i\}_{i=1}^N$,

$$V_{\text{ms},\ell} := \text{span} \left\{ \chi_i \mathcal{L}_i^{-1}(\psi_{i,\ell}^j) : 1 \leq i \leq N \text{ and } 1 \leq j \leq 2^{\ell+2} \right\}. \quad (3.12)$$

We summarize the construction of edge multiscale ansatz space in Algorithm 1.

Algorithm 1: Edge Multiscale ansatz space

Data: The level parameter $\ell \in \mathbb{N}$; coarse neighborhood ω_i and its four coarse edges Γ_i^k with $k = 1, 2, 3, 4$; the subspace $E_{i,\ell}^k \subset L^2(\Gamma_i^k)$ up to level ℓ on each coarse edge Γ_i^k .

Result: $V_{\text{ms},\ell}$

- 1 Construct the local edge space $E_{i,\ell}$ (3.9);
 - 2 Calculate the local multiscale space $\mathcal{L}_i^{-1}(E_{i,\ell})$ (3.10);
 - 3 Construct the global multiscale space $V_{\text{ms},\ell}$ (3.12).
-

Once the local multiscale basis functions are identified, we solve for $u_{\text{ms},\ell}(\cdot, t) \in V_{\text{ms},\ell}$, such that

$$\begin{aligned} (\partial_t u_{\text{ms},\ell}, v) + A(u_{\text{ms},\ell}, v) &= (R(\cdot, u_{\text{ms},\ell}), v), \quad \text{for each } v \in V_{\text{ms},\ell}, \\ u_{\text{ms}}(\cdot, 0) &= \mathcal{I}_\ell u_0. \end{aligned} \quad (3.13)$$

Here, $\mathcal{I}_\ell : L^2(D) \rightarrow V_{\text{ms},\ell}$ denotes the L^2 -projection.

To obtain the convergence rates of (3.13), we introduce the global projection operator \mathcal{P}_ℓ of level $\ell : V \rightarrow V_{\text{ms},\ell}$. Since the edge multiscale ansatz space $V_{\text{ms},\ell}$ is generated by the local multiscale space $\mathcal{L}_i^{-1}(E_{i,\ell})$ using the partition of unity (3.12), we only need to define the local interpolation operator $\mathcal{P}_{i,\ell} : C(\partial\omega_i) \rightarrow \mathcal{L}^{-1}(E_{i,\ell})$. Let $\mathcal{I}_{i,\ell} : L^2(\partial\omega_i) \rightarrow E_{i,\ell}$ be the L^2 -projection, then we define $\mathcal{P}_{i,\ell} : L^2(\partial\omega_i) \rightarrow \mathcal{L}^{-1}(E_{i,\ell})$ by

$$\mathcal{P}_{i,\ell} v := \mathcal{L}_i^{-1}(\mathcal{I}_{i,\ell} v|_{\partial\omega_i}).$$

Observe that any $v \in V$ can be expressed by

$$v = \sum_{i=1}^N \chi_i v|_{\omega_i}.$$

Then the global interpolation \mathcal{P}_ℓ of level ℓ is defined by means of the local projection,

$$\mathcal{P}_\ell v := \sum_{i=1}^N \chi_i (\mathcal{P}_{i,\ell} v), \quad \text{for each } v \in V. \quad (3.14)$$

3.5 Error estimates

In this section, we are concerned with deriving the convergence rates of (3.13) following the framework given in Li (2019); Fu et al. (2023). The following result is a slight modification of Lemma 5.1 from Fu et al. (2023), which establishes *a priori* estimates for the global bubble function u^I .

Lemma 3.2. *Let u^I be defined in (3.7). Then there holds*

$$\|u^I\|_{L^2(D)} + H\|\nabla u^I\|_{L_\kappa^2(D)} \leq H^2 (\|u\|_{H^1(D)} + \|\partial_t u\|_{L^2(D)}). \quad (3.15a)$$

Proof. First, we multiply (3.4) by $u^{i,I}$ and integrate over ω_i to obtain

$$\int_{\omega_i} \kappa |\nabla u^{i,I}|^2 dx + \int_{\omega_i} (\beta \cdot \nabla u^{i,I}) u^{i,I} dx = \int_{\omega_i} (R(x, u) - \partial_t u) u^{i,I} dx,$$

using the fact $u^{i,I}|_{\partial\omega_i} = 0$, we reduce the expression above to

$$\int_{\omega_i} \kappa |\nabla u^{i,I}|^2 dx = \int_{\omega_i} (R(x, u) - \partial_t u) u^{i,I} dx.$$

Combining the Schwarz inequality and the Friedrich's inequality, we arrive at

$$\|\nabla u^{i,I}\|_{L_\kappa^2(\omega_i)}^2 \leq \frac{\sqrt{2}H}{\pi} \|R(\cdot, u) - \partial_t u\|_{L^2(\omega_i)} \|\nabla u^{i,I}\|_{L_\kappa^2(\omega_i)}.$$

Since $R(x, 0) = 0$, together with Lemma 2.3, we obtain that

$$\|\nabla u^{i,I}\|_{L_\kappa^2(\omega_i)} \leq CH (\|u\|_{H^1(\omega_i)} + \|\partial_t u\|_{L^2(\omega_i)}).$$

Next, we obtain the desired assertion by invoking Friedrich's inequality and the overlapping condition (3.1). \square

Now, we introduce the approximation properties of the global interpolation operator \mathcal{P}_ℓ .

Lemma 3.3. *Let $d = 2, 3$, and $s > 0$. Assume that the level parameter ℓ is non-negative. Let $u \in V$ solve problem (2.1) and define the global Harmonic extension u^{II} in (3.7). Then, there holds*

$$\|u^{\text{II}} - \mathcal{P}_\ell u^{\text{II}}\|_{L_\kappa^2(D)} \preceq \eta(H, \ell, s) H \|u\|_{H^{s+1/2}(D)}, \quad (3.16a)$$

$$\|\nabla(u^{\text{II}} - \mathcal{P}_\ell u^{\text{II}})\|_{L_\kappa^2(D)} \preceq \eta(H, \ell, s) \|u\|_{H^{s+1/2}(D)}. \quad (3.16b)$$

Here,

$$\eta(H, \ell, s) := \|\kappa\|_{L^\infty(\mathcal{F}_H)}^{1/2} 2^{-s\ell} H^{s+d/2-1}. \quad (3.17)$$

Proof. First, the property of the partition of unity of $\{\chi_i\}_{i=1}^N$ along with expression (3.7) yields

$$u^\Pi - \mathcal{P}_\ell u^\Pi = \sum_{i=1}^N \chi_i (u^{i,\Pi} - \mathcal{P}_{i,\ell} u^{i,\Pi}).$$

Using the rescaling argument and Proposition 3.1, we obtain

$$\|u^{i,\Pi} - \mathcal{P}_{i,\ell} u^{i,\Pi}\|_{L^2(\partial\omega_i)} \leq C 2^{-s\ell} H^s |u^{i,\Pi}|_{H^s(\partial\omega_i)},$$

By definition, $u^{i,\Pi} = u$ on $\partial\omega_i$, together with the trace inequality, this implies

$$\|u^{i,\Pi} - \mathcal{P}_{i,\ell} u^{i,\Pi}\|_{L^2(\partial\omega_i)} \leq C 2^{-s\ell} H^s \|u\|_{H^{s+1/2}(\omega_i)}. \quad (3.18)$$

Following similar steps as in (Li, 2019, The proof to Theorem A.1, pp. 615), we can prove

$$\begin{aligned} \|u^{i,\Pi} - \mathcal{P}_{i,\ell} u^{i,\Pi}\|_{L^2_\kappa(\omega_i)} &\leq C H^{d/2} \|u^{i,\Pi} - \mathcal{P}_{i,\ell} u^{i,\Pi}\|_{L^2_\kappa(\partial\omega_i)} \\ &\leq C H^{d/2} \|\kappa\|_{L^\infty(\partial\omega_i)}^{1/2} \|u^{i,\Pi} - \mathcal{P}_{i,\ell} u^{i,\Pi}\|_{L^2(\partial\omega_i)}. \end{aligned}$$

This, together with (3.18), leads to

$$\|u^{i,\Pi} - \mathcal{P}_{i,\ell} u^{i,\Pi}\|_{L^2_\kappa(\omega_i)} \leq C 2^{-s\ell} H^{s+d/2} \|\kappa\|_{L^\infty(\partial\omega_i)}^{1/2} \|u\|_{H^{s+1/2}(\omega_i)}. \quad (3.19)$$

By a standard Caccioppoli type inequality, see, e.g., (Li, 2019, Proof to Lemma 4.4), we derive

$$\|\chi_i \nabla(u^{i,\Pi} - \mathcal{P}_{i,\ell} u^{i,\Pi})\|_{L^2_\kappa(\omega_i)} \leq C 2^{-s\ell} H^{s+d/2-1} \|\kappa\|_{L^\infty(\partial\omega_i)}^{1/2} \|u\|_{H^{s+1/2}(\omega_i)}. \quad (3.20)$$

Invoking the overlapping condition (3.1) and (3.19), leads to

$$\begin{aligned} \|u^\Pi - \mathcal{P}_\ell u^\Pi\|_{L^2_\kappa(D)} &\leq \sqrt{C_{\text{ov}}} C_\infty \left(\sum_{i=1}^N \|u^{i,\Pi} - \mathcal{P}_{i,\ell} u^{i,\Pi}\|_{L^2_\kappa(\omega_i)}^2 \right)^{1/2} \\ &\leq 2^{-s\ell} H^{s+d/2} \|\kappa\|_{L^\infty(\mathcal{F}_H)}^{1/2} \|u\|_{H^{s+1/2}(D)}. \end{aligned}$$

This proves (3.16a).

Next, applying the overlapping condition (3.1) again, we obtain

$$\begin{aligned} \|\nabla(u^{i,\Pi} - \mathcal{P}_{i,\ell} u^{i,\Pi})\|_{L^2_\kappa(D)} &\leq \sqrt{2C_{\text{ov}}} \left(\sum_{i=1}^N C_G^2 H^{-2} \|u^{i,\Pi} - \mathcal{P}_{i,\ell} u^{i,\Pi}\|_{L^2_\kappa(\omega_i)}^2 \right. \\ &\quad \left. + \|\chi_i \nabla(u^{i,\Pi} - \mathcal{P}_{i,\ell} u^{i,\Pi})\|_{L^2_\kappa(\omega_i)}^2 \right)^{1/2}. \end{aligned} \quad (3.21)$$

Combining with (3.19) and (3.20) reveals the second assertion. This completes the proof. \square

Let \mathcal{R}_ℓ be the elliptic projection operator in the multiscale space $V_{\text{ms},\ell}$, *i.e.*,

$$\text{for each } v \in V \text{ and } w_{\text{ms},\ell} \in V_{\text{ms},\ell} : A(v - \mathcal{R}_\ell v, w_{\text{ms},\ell}) = 0. \quad (3.22)$$

Lemma 3.4. *Let ℓ be a non-negative integer and $s > 0$. Let u be the solution to problem (2.1). Then there holds*

$$\begin{aligned} \|\nabla(u - \mathcal{R}_\ell u)\|_{L^2_\kappa(D)} + \|u - \mathcal{R}_\ell u\|_{L^2(D)} &\lesssim \eta(H, \ell, s) \|u\|_{H^{s+1/2}(D)} \\ &+ H \left(\|u\|_{H^1(D)} + \|\partial_t u\|_{L^2(D)} \right). \end{aligned} \quad (3.23)$$

Proof. We obtain from the global decomposition (3.6), (2.6) and (3.22),

$$\|\nabla(u - \mathcal{R}_\ell u)\|_{L^2_\kappa(D)}^2 = A(u - \mathcal{R}_\ell u, u - \mathcal{R}_\ell u) \leq A(u - \mathcal{R}_\ell u, u^I + e^{\text{II}}).$$

Here, $e^{\text{II}} := u^{\text{II}} - \mathcal{P}_\ell u^{\text{II}}$. The definition of the bilinear form $A(\cdot, \cdot)$, together with the Cauchy-Schwarz inequality, further leads to

$$\begin{aligned} \|\nabla(u - \mathcal{R}_\ell u)\|_{L^2_\kappa(D)}^2 &= \int_D \kappa \nabla(u - \mathcal{R}_\ell u) \cdot \nabla(u^I + e^{\text{II}}) dx + \int_D \beta \cdot \nabla(u - \mathcal{R}_\ell u)(u^I + e^{\text{II}}) dx \\ &\leq \|\nabla(u - \mathcal{R}_\ell u)\|_{L^2_\kappa(D)} \|\nabla(u^I + e^{\text{II}})\|_{L^2_\kappa(D)} \\ &\quad + \|\beta\|_{L^\infty(D)} \|\nabla(u - \mathcal{R}_\ell u)\|_{L^2(D)} \|u^I + e^{\text{II}}\|_{L^2(D)}. \end{aligned}$$

Since $\kappa \geq 1$, we derive

$$\|\nabla(u - \mathcal{R}_\ell u)\|_{L^2_\kappa(D)} \leq \|\nabla(u^I + e^{\text{II}})\|_{L^2_\kappa(D)} + \|u^I + e^{\text{II}}\|_{L^2(D)}.$$

Finally, an application of Lemma 3.2, Lemma 3.3, and Friedrich's inequality yields the desired assertion. \square

Since $u_0 \in \dot{H}^2(D)$, similar argument as the proof to Lemma 3.4 leads to

$$\|\nabla(u_0 - \mathcal{R}_\ell u_0)\|_{L^2_\kappa(D)} + \|u_0 - \mathcal{R}_\ell u_0\|_{L^2(D)} \lesssim \eta(H, \ell, s) \|u_0\|_{H^{s+1/2}(D)} + H \|\mathcal{L}u_0\|_{L^2(D)}. \quad (3.24)$$

Finally, We present an estimate for the semi-discrete formulation given in (3.13), which follows from (Thomée, 2006, Theorem 14.2, pp. 246), together with Lemma 3.4 and (3.24).

Theorem 3.5. *Let ℓ be a non-negative integer, $s > 0$ and $u_0 \in \dot{H}^2(D)$. Let u and $u_{\text{ms},\ell}$ be the solutions to Problem (2.1) and Problem (3.13), respectively. There holds*

$$\begin{aligned} \|\nabla(u(t) - u_{\text{ms},\ell}(t))\|_{L^2_\kappa(D)} + \|u(t) - u_{\text{ms},\ell}(t)\|_{L^2(D)} \\ \leq \eta(H, \ell, s) \left(\|u(t)\|_{H^{s+1/2}(D)} + \|u_0\|_{H^{s+1/2}(D)} \right) \\ + H \left(\|u(t)\|_{H^1(D)} + \|\partial_t u(t)\|_{L^2(D)} + \|\mathcal{L}u_0\|_{L^2(D)} \right), \end{aligned}$$

for all $t \in (0, T]$.

4 Full discretization

In this section, we introduce the fully discrete scheme of (2.5) based on exponential integration techniques Hochbruck et al. (1998); Hochbruck and Ostermann (2005, 2010). The effectiveness of these approaches is attributed to the computation of the matrix-valued exponential integrator. Their prominence has increased in the past decade due to advancements in numerical linear algebra and efficient algorithms for computing these functions (Caliari et al., 2024; Caliari and Cassini, 2024). Consequently, these methods have become significantly more competitive, offering an alternative to traditional temporal discretizations.

Let $0 = t^0 < t^1 < \dots < t^{N_t-1} < t^{N_t} = T$ be a uniform partition of the interval $[0, T]$, with the time-step size given by $\Delta t = \max_{n=1, \dots, N_t} \{t^n - t^{n-1}\}$, where N_t is a positive integer. We recall exponential integration techniques relevant to the proposed multiscale finite element method.

First, we define the discrete solution $u_{\text{ms},\ell}(t)$ evolving in time. Since that $A(\cdot, \cdot)$ is bounded and coercive over $V_{\text{ms},\ell} \times V_{\text{ms},\ell}$, then Riesz's representation Theorem implies the existence of a bounded linear operator $L_{\text{ms}} : V_{\text{ms},\ell} \rightarrow V'_{\text{ms},\ell}$, satisfying

$$A(u_{\text{ms},\ell}, v_{\text{ms},\ell}) = \langle L_{\text{ms}} u_{\text{ms},\ell}, v_{\text{ms},\ell} \rangle, \quad \text{for each } v_{\text{ms},\ell} \in V_{\text{ms},\ell}. \quad (4.1)$$

Here, $\langle \cdot, \cdot \rangle$ denote the duality paring. Then we can rewrite (2.5) in a semidiscrete formulation in $V_{\text{ms},\ell}$

$$\begin{aligned} \partial_t u_{\text{ms},\ell} + L_{\text{ms}} u_{\text{ms},\ell} &= P_{\text{ms}} R(\cdot, u_{\text{ms},\ell}), \quad t \in (0, T], \\ u_{\text{ms},\ell}(0) &= P_{\text{ms}} u_0, \end{aligned} \quad (4.2)$$

where $P_{\text{ms}} : L^2(D) \rightarrow V_{\text{ms},\ell}$ denotes L^2 -projection.

Following Henry (1981), the V-elliptic property of L_{ms} implies that $-L_{\text{ms}}$ is a sectorial on $L^2(D)$ (uniformly in h), *i.e.*, there exist $C > 0$ and $\theta \in (\frac{1}{2}\pi, \pi)$ such that

$$\|(\lambda I + L_{\text{ms}})^{-1}\|_{L(L^2(D), L^2(D))} \leq \frac{C}{|\lambda|}, \quad \lambda \in S_\theta,$$

where $S_\theta := \{\lambda \in \mathbb{C} : \lambda = \rho e^{i\phi}, \rho > 0, 0 \leq \phi \leq \theta\}$. The discrete operator is the infinitesimal of the exponential operator $e^{-tL_{\text{ms}}}$ on $V_{\text{ms},\ell}$ such that

$$e^{-tL_{\text{ms}}} := \frac{1}{2\pi} \int_{\Gamma} e^{t\lambda} (\lambda I + L_{\text{ms}})^{-1} d\lambda, \quad t > 0,$$

where Γ represents a path surrounding the spectrum of $-L_{\text{ms}}$. According to Duhamel's principle, we ensure the existence and uniqueness of the solution, which is given by the integral form

$$u_{\text{ms},\ell}(t^{n+1}) = e^{-\Delta t L_{\text{ms}}} u_{\text{ms},\ell}(t^n) + \int_0^{\Delta t} e^{-(\Delta t-s)L_{\text{ms}}} P_{\text{ms}} R(\cdot, u_{\text{ms},\ell}(t^n + s)) ds. \quad (4.3)$$

Approximating $u_{\text{ms},\ell}(t^n + s)$ by $u_{\text{ms},\ell}(t^n)$ for $s \in [0, \Delta t]$ (Hochbruck and Ostermann, 2010), we can obtain a fully discrete multiscale method for Problem (3.13) as follows: for $n = 0, \dots, N_t - 1$,

$$u_{\text{ms},\ell}^{n+1} = e^{-\Delta t L_{\text{ms}}} u_{\text{ms},\ell}^n + L_{\text{ms}}^{-1} (I - e^{-\Delta t L_{\text{ms}}}) P_{\text{ms}} R(\cdot, u_{\text{ms},\ell}^n).$$

Together with the fact $e^{-\Delta t L_{\text{ms}}} = -\Delta t L_{\text{ms}} \phi_1(-\Delta t L_{\text{ms}}) + I$ with $\phi_1(z) = \frac{e^z - I}{z}$, this implies

$$u_{\text{ms},\ell}^{n+1} = u_{\text{ms},\ell}^n + \Delta t \phi_1(-\Delta t L_{\text{ms}}) (P_{\text{ms}} R(\cdot, u_{\text{ms},\ell}^n) - L_{\text{ms}} u_{\text{ms},\ell}^n), \quad (4.4)$$

which is the so-called exponential Euler scheme. Note that this scheme involves huge computational complexity when applied to (2.1) directly using standard numerical methods such as the finite element method, due to the existence of heterogeneous coefficient κ and the evaluation of the exponential-like matrix function $\phi_1(\cdot)$. In sharp contrast, our proposed edge multiscale method (3.13) offers a significant advantage. It reduces the size of the exponential-like matrix function $\phi_1(\cdot)$, thereby making exponential integration feasible even for such challenging multiscale problems.

The following result will be mainly used in this work.

Proposition 4.1 (Properties of the semigroup Henry, 1981). *Let $\alpha \geq 0$ and any given parameter $0 \leq \gamma \leq 1$, then there exists a constant $C > 0$ such that*

$$\begin{aligned} \|L_{\text{ms}}^\alpha e^{-t L_{\text{ms}}}\|_{L^2(D)} &\leq C t^{-\alpha}, \quad \text{for } t > 0, \\ \|L_{\text{ms}}^{-\gamma} (I - e^{-t L_{\text{ms}}})\|_{L^2(D)} &\leq C t^\gamma, \quad \text{for } t \geq 0. \end{aligned}$$

4.1 Error estimates

This subsection concerns the convergence study of fully discrete scheme (4.4).

Theorem 4.2. *Let ℓ be a non-negative integer, $s > 0$ and $u_0 \in \dot{H}^2(D)$. Let $u \in V$ and $u_{\text{ms},\ell}^n$ be the solution to Problems (2.1) and (4.4), respectively. When the stepping size Δt is sufficiently small, there holds*

$$\begin{aligned} \|u(t^n) - u_{\text{ms},\ell}^n\|_{L^2(D)} &\preceq \eta(H, \ell, s) \left(\|u(t)\|_{H^{s+1/2}(D)} + \|u_0\|_{H^{s+1/2}(D)} \right) \\ &\quad + H \left(\|u(t)\|_{H^1(D)} + \|\partial_t u(t)\|_{L^2(D)} + \|\mathcal{L}u_0\|_{L^2(D)} \right) + \Delta t. \\ \|\nabla(u(t^n) - u_{\text{ms},\ell}^n)\|_{L_\kappa^2(D)} &\preceq \eta(H, \ell, s) \left(\|u(t)\|_{H^{s+1/2}(D)} + \|u_0\|_{H^{s+1/2}(D)} \right) \\ &\quad + H \left(\|u(t)\|_{H^1(D)} + \|\partial_t u(t)\|_{L^2(D)} + \|\mathcal{L}u_0\|_{L^2(D)} \right) + \Delta t (t^n)^{-1/2}. \end{aligned}$$

Here, the hidden constant may depend on $R, \beta, u, \partial_t u, \partial_{tt}^2 u$, and T .

Proof. The proof to the first estimate is similar to (Tambue, 2016, proof to Theorem 4.1). To obtain the second estimate, an application of the triangle inequality yields

$$\begin{aligned} \|\nabla(u(t^n) - u_{\text{ms},\ell}^n)\|_{L_{\kappa}^2(D)} &\leq \|\nabla(u(t^n) - u_{\text{ms},\ell}(t^n))\|_{L_{\kappa}^2(D)} + \|\nabla(u_{\text{ms},\ell}(t^n) - u_{\text{ms},\ell}^n)\|_{L_{\kappa}^2(D)} \\ &:= I_1 + I_2. \end{aligned}$$

From Theorem 3.5, we get an upper bound for the first term I_1 . Thus, our focus is on the second term I_2 . Note that the integral form of the semidiscrete solution $u_{\text{ms},\ell}$ (4.3) and its approximation $u_{\text{ms},\ell}^n$ (4.4) indicate,

$$\begin{aligned} u_{\text{ms},\ell}(t^n) &= e^{-\Delta t L_{\text{ms}}} u_{\text{ms},\ell}(0) + \sum_{k=0}^{n-1} \int_{t^k}^{t^{k+1}} e^{-(t^n-s)L_{\text{ms}}} P_{\text{ms}} R(\cdot, u_{\text{ms},\ell}(s)) ds, \\ u_{\text{ms},\ell}^n &= e^{-\Delta t L_{\text{ms}}} u_{\text{ms},\ell}(0) + \sum_{k=0}^{n-1} \int_{t^k}^{t^{k+1}} e^{-(t^n-s)L_{\text{ms}}} P_{\text{ms}} R(\cdot, u_{\text{ms},\ell}^k) ds. \end{aligned}$$

Hence, subtracting the second equation from the first one, we obtain the temporal discretization error,

$$\varepsilon_{\text{ms},\ell}^n := u_{\text{ms},\ell}(t^n) - u_{\text{ms},\ell}^n = \sum_{k=0}^{n-1} \int_{t^k}^{t^{k+1}} e^{-(t^n-s)L_{\text{ms}}} P_{\text{ms}} \left(R(\cdot, u_{\text{ms},\ell}(s)) - R(\cdot, u_{\text{ms},\ell}^k) \right) ds.$$

Then, together with the triangle inequality and the equivalence of norms, see, e.g. (Henry, 1981, Theorem 1.4.6),

$$\|\nabla v_{\text{ms},\ell}\|_{L_{\kappa}^2(D)} \simeq \|L_{\text{ms}}^{1/2} v_{\text{ms},\ell}\|_{L^2(D)}, \quad \text{for each } v_{\text{ms},\ell} \in \mathbb{V}_{\text{ms},\ell},$$

this leads to

$$\begin{aligned} \|\nabla \varepsilon_{\text{ms},\ell}^n\|_{L_{\kappa}^2(D)} &\leq \sum_{k=0}^{n-1} \int_{t^k}^{t^{k+1}} \left\| \nabla e^{-(t^n-s)L_{\text{ms}}} P_{\text{ms}} \left(R(\cdot, u_{\text{ms},\ell}(s)) - R(\cdot, u_{\text{ms},\ell}^k) \right) \right\|_{L_{\kappa}^2(D)} ds \\ &\simeq \sum_{k=0}^{n-1} \int_{t^k}^{t^{k+1}} \left\| e^{-(t^n-s)L_{\text{ms}}} L_{\text{ms}}^{1/2} P_{\text{ms}} \left(R(\cdot, u_{\text{ms},\ell}(s)) - R(\cdot, u_{\text{ms},\ell}^k) \right) \right\|_{L^2(D)} ds. \end{aligned}$$

Since P_{ms} is the L^2 -projection, we get therefore,

$$\|\nabla \varepsilon_{\text{ms},\ell}^n\|_{L_{\kappa}^2(D)} \leq \sum_{k=0}^{n-1} \int_{t^k}^{t^{k+1}} \left\| e^{-(t^n-s)L_{\text{ms}}} L_{\text{ms}}^{1/2} \right\|_{L^2(D)} \left\| R(\cdot, u_{\text{ms},\ell}(s)) - R(\cdot, u_{\text{ms},\ell}^k) \right\|_{L^2(D)} ds.$$

The remaining proof is similar to (Tambue, 2016, proof to Theorem 4.1). \square

5 Numerical tests

In this section, we present several numerical tests to demonstrate the accuracy of Scheme (4.4). To obtain a reference solution with sufficient accuracy, we set the fine-scale mesh size of $h = 2^{-9}$ for $d = 2$ and $h = 2^{-6}$ for $d = 3$. Moreover, we take $h = 2^{-8}$ in Example 5.4 of 2-d two-component coupled systems. The backward Euler method is utilized for temporal discretization for the reference solution. A Homogeneous Dirichlet boundary condition is imposed for all tests.

The functions χ_i are the standard multiscale basis functions on each coarse element $K \in \mathcal{T}_H$ defined by

$$\begin{cases} -\nabla \cdot (\kappa \nabla \chi_i) = 0, & \text{in } K, \\ \chi_i = g_i, & \text{on } \partial K, \end{cases} \quad (5.1)$$

where g_i is affine over ∂K with $g_i(x_j) = \delta_{ij}$ for all $i, j = 1, \dots, N$. Recall that $\{x_j\}_{j=1}^N$ are the set of coarse nodes on \mathcal{T}_H .

To measure the approximation accuracy, we consider the following notation for the relative errors in L^2 - and H_κ^1 -norm and the numerical convergence rate CR:

$$\varepsilon_0 = \frac{\|u_h^N - u_{\text{ms},\ell}^N\|_{L^2(D)}}{\|u_h^N\|_{L^2(D)}}, \quad \varepsilon_1 = \frac{\|\nabla(u_h^N - u_{\text{ms},\ell}^N)\|_{L_\kappa^2(D)}}{\|\nabla u_h^N\|_{L_\kappa^2(D)}}, \quad \text{CR} = \frac{|\ln \varepsilon_\star^H - \ln \varepsilon_\star^{H/2}|}{\ln 2},$$

where u_h^N and u_{ms}^N denotes the reference and multiscale solution at final time $t = T$ respectively. ε_\star^H denotes the relative error with coarse mesh size H , for $\star \in \{0, 1\}$. Consequently, CR measures the convergence rate in H . In addition, we shall evaluate (4.4) via Padé approximations implemented via EXPINT package in Berland et al. (2007).

Example 5.1. First, we consider the 2-d convective Allen-Cahn problem,

$$\partial_t u - \nabla \cdot (\kappa \nabla u) + \beta \cdot \nabla u = \frac{1}{\epsilon^2}(u - u^3), \quad \text{in } D \times (0, T], \quad (5.2)$$

where $\epsilon = 0.1$ measures the interface thickness, $D = [-1, 1]^2$, and $T = 1$ and time step size of $\Delta t = 2^{-10}$. The diffusion coefficient $\kappa = 1$ and the incompressible velocity field is $\beta := e^{-t}(\cos(2\pi y), \cos(2\pi x))^T$. The initial data is $u_0 := \sin(2\pi x) \sin(2\pi y)$.

Table 1 reports the numerical results of (4.4) with level parameter $\ell = 0, 1, 2$ and varying coarse grid size $H = 2^{-j}$, where $j \in \{1, \dots, 5\}$. We observe that its accuracy improves as the coarse grid size H decreases and the level parameter ℓ increases. In addition, all levels have a rate of convergence close to 1 with time-stepping fixed, which coincides with the theoretical results given in Theorem 4.2. Figure 2 depicts the snapshots of the reference and multiscale solution with $\ell = 1$ and $H = 2^{-4}$ and different time steps at $t = 0, 0.0098, 0.125$ and 0.75 .

In Table 2, we present the relative errors and their corresponding convergence rates for $\ell = 1$, where the temporal convergence rates are much better than expected (higher than

Multiscale approximation at $T = 1$						
H	$\ell = 0$		$\ell = 1$		$\ell = 2$	
	ε_0	CR	ε_0	CR	ε_0	CR
2^{-1}	1.0638E+00	–	2.4791E-02	–	1.5226E-02	–
2^{-2}	4.4884E-02	4.5669	9.2118E-03	1.4283	4.0592E-03	1.9073
2^{-3}	4.3052E-03	3.3821	1.2737E-03	2.8544	6.5153E-04	2.6393
2^{-4}	1.5135E-03	1.5081	3.0049E-04	2.0836	2.7358E-05	4.5738
2^{-5}	2.3453E-04	2.6901	4.8751E-05	2.6238	4.6474E-06	2.5575

Table 1: Relative errors and convergence rates for Example 5.1 at $T = 1$ with varying parameters (H, ℓ) .

Multiscale approximation at $T = 0.01$					
H	Δt	ε_0	CR	ε_1	CR
2^{-2}	2^{-5}	2.0231E-02	–	2.0231E-02	–
2^{-3}	2^{-6}	1.3950E-02	0.5363	1.3950E-02	6.4657E-01
2^{-4}	2^{-7}	5.8310E-03	1.2584	5.8310E-03	1.7156E+00
2^{-5}	2^{-8}	7.5210E-04	2.9547	7.5210E-04	2.1164E+00

Table 2: Relative errors and convergence rates in time, for Example 5.1 at $T = 0.01$ decreasing simultaneously the time step size Δt and the coarse size H with $\ell = 1$.

1) from theoretical results given in Theorem 4.2. We mention that for a fixed coarse size H , the convergence rate in time degrades as the spatial error gradually dominates the total error.

We present in Figure 3 the corresponding evolution of the classic free energy \mathcal{E} (see, for instance, Bartels, 2015) defined by

$$\mathcal{E}[u] := \int_D \left(\frac{1}{2} |\nabla u|^2 + \frac{1}{4\epsilon^2} (u^2 - 1)^2 \right) dx,$$

and max-norm of the multiscale solution using $H = 2^{-4}$ and $\ell = 1$. We observe monotone decay of the discrete energy over time, and the discrete maximum principle is well-preserved.

Example 5.2. Next, we investigate the performance of the proposed method for the

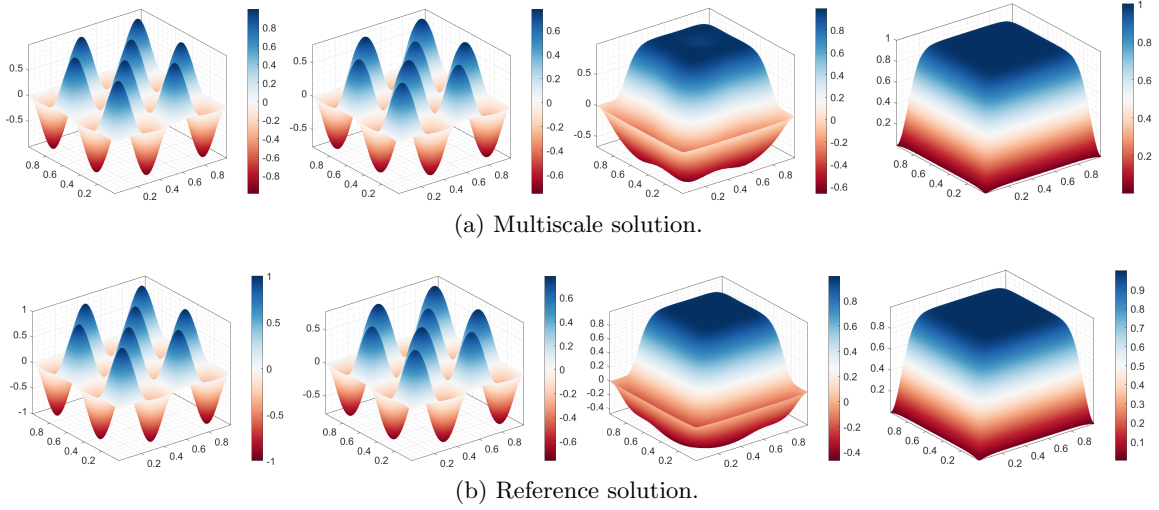


Figure 2: Solutions of Example 5.1 at $t = 0, 0.098, 0.125$ and 0.750 (a) Multiscale solution with $H = 2^{-4}$ and $\ell = 1$, and (b) the reference solution.

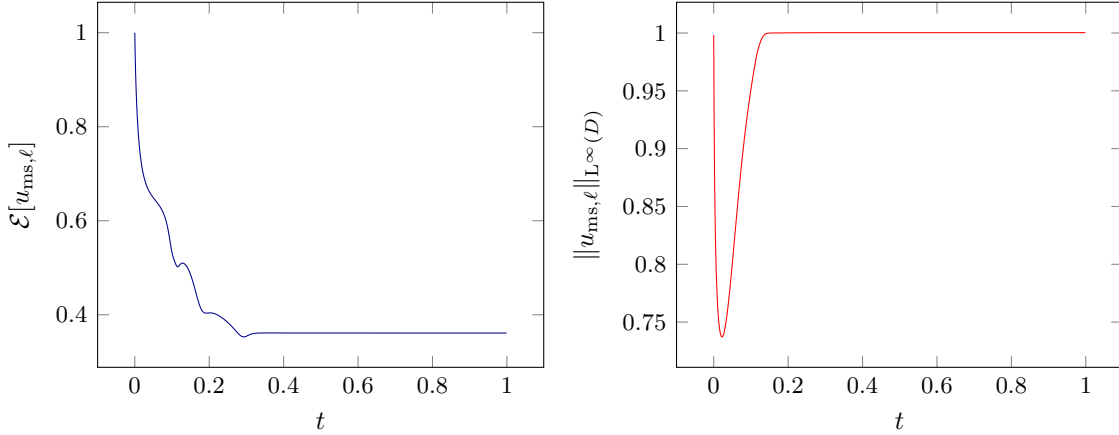


Figure 3: Time-dependent normalized discrete total energy (left) and maximum values of the multiscale solution $u_{\text{ms},\ell}$ (right) over time evolution with $\Delta t = 2^{-10}$ in Example 5.1.

convective Allen-Cahn problem with heterogeneous coefficient,

$$\partial_t u - \nabla \cdot (\kappa_2 \nabla u) + \beta \cdot \nabla u = \frac{1}{\epsilon^2} (u - u^3), \quad \text{in } D \times (0, T], \quad (5.3)$$

where $D = [0, 1]^2$, $T = 0.016$, and $\epsilon = 0.05$. The heterogeneous coefficient κ_2 is depicted in Figure 4b, which takes value 1 in the background (gray region) and 10^4 in other parts (red region).

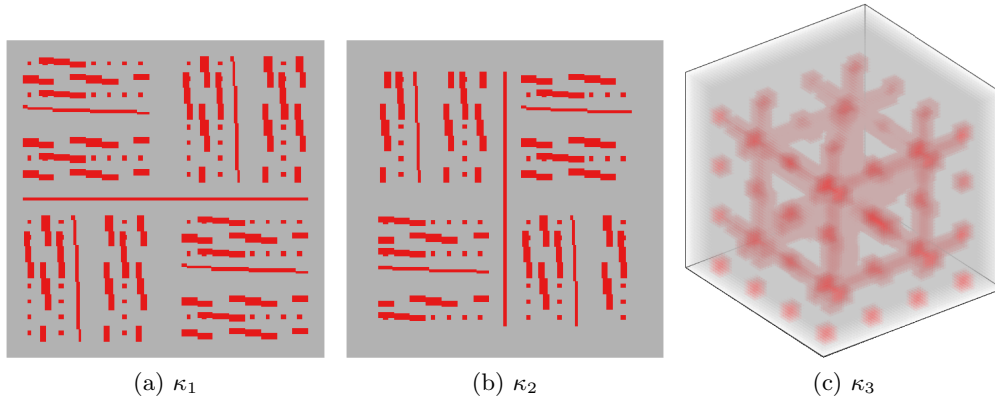


Figure 4: Permeability fields (color online).

We set the velocity term as

$$\beta = \alpha(\cos(k\pi y) \sin(k\pi x), -\cos(k\pi x) \sin(k\pi y))^T,$$

where $\alpha = 2$ and $k = 24$. The initial data is $u_0 := 0.1 \sin(\pi x) \sin(\pi y)$.

Table 3 exhibits convergence history of (4.4) with varying coarse grid size $H = 2^{-j}$, where $j \in \{1, \dots, 5\}$ and the level parameter of $\ell = 0, 1, 2$. We observe convergence as the coarse grid size H decreases and level parameter ℓ increases, which agrees with Example 5.2. Figure 5 depicts the snapshots of the multiscale solution with $\ell = 2$ and $H = 2^{-4}$, and reference solutions at $t = 0, 1.5625\text{E-}04, 0.004$ and 0.012 .

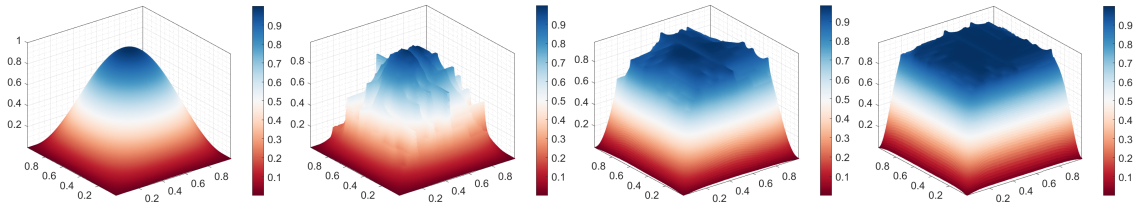
Multiscale approximation at $T = 0.016$						
H	$\ell = 0$		$\ell = 1$		$\ell = 2$	
	ε_0	CR	ε_0	CR	ε_0	CR
2^{-1}	1.0748E-01	–	3.4636E-02	–	1.0946E-02	–
2^{-2}	5.3665E-02	1.0020	1.0082E-02	1.7805	4.4932E-03	1.2846
2^{-3}	1.2131E-02	2.1453	3.6757E-03	1.4557	1.7822E-03	1.3341
2^{-4}	5.6863E-03	1.0931	1.3696E-03	1.4243	3.3765E-04	2.4001
2^{-5}	3.1386E-03	0.8574	3.1399E-04	2.1250	6.5368E-05	2.3689

Table 3: Relative errors and convergence rates for Example 5.2 at $T = 0.016$ with varying parameters (H, ℓ) .

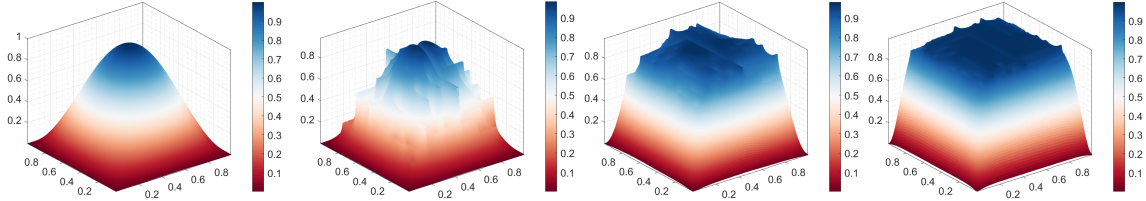
In Table 4, we present the relative errors and their corresponding convergence rates for

Multiscale approximation at $T = 0.016$					
H	Δt	ε_0	CR	ε_1	CR
2^{-2}	2^{-5}	1.0082E-02	–	2.0231E-02	–
2^{-3}	2^{-6}	3.6751E-03	1.4559E+00	1.3950E-02	9.7428E-01
2^{-4}	2^{-7}	1.3686E-03	1.4251E+00	5.8310E-03	8.5800E-01
2^{-5}	2^{-8}	3.1213E-04	2.1325E+00	7.5210E-04	1.2340E+00

Table 4: Relative errors and convergence rates in time, for Example 5.2 at $T = 0.016$ decreasing simultaneously the time step size Δt and the coarse size H with $\ell = 1$.



(a) Multiscale solution.



(b) Reference solution.

Figure 5: Solutions of Example 5.2 at $t = 0, 1.5625\text{E-}04, 0.004$ and 0.012 (a) Multiscale solution with $H = 2^{-4}$ and $\ell = 2$, and (b) the reference solution.

$\ell = 1$, where the temporal convergence rates are much faster than expected (higher than 1) from theoretical results given in Theorem 4.2. As mentioned in Example 5.1, for a fixed coarse size H , the convergence rate in time also degrades as the spatial error gradually dominates the total error.

We present in Figure 6 the evolution of the classic free energy \mathcal{E} and max-norm of the multiscale solution of Example 5.2. Again, it is observed that the discrete energy decays monotonically over time, and the discrete maximum principle is preserved.

Example 5.3. In this numerical example, we consider a 3-d convective Allen-Cahn problem,

$$\partial_t u - \nabla \cdot (\kappa_3 \nabla u) + \beta \cdot \nabla u = \frac{1}{\varepsilon^2} (u - u^3), \quad \text{in } D \times (0, T], \quad (5.4)$$

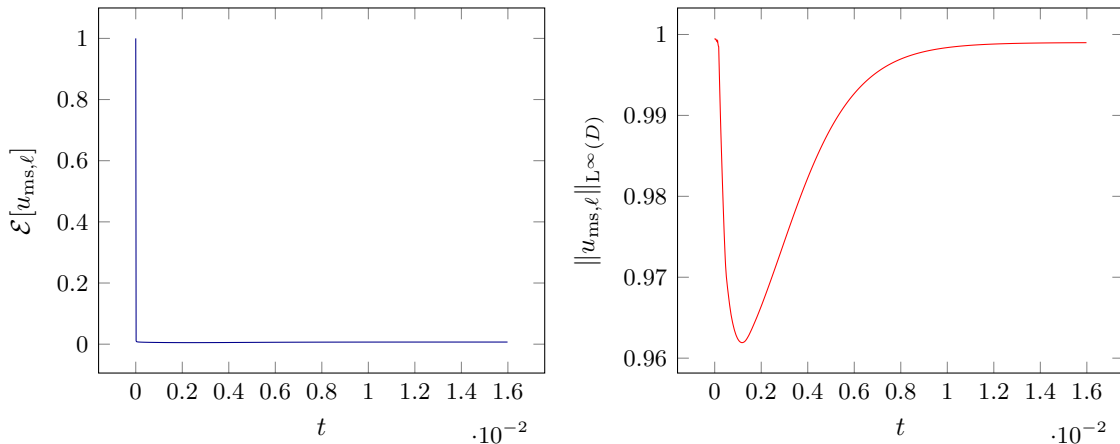


Figure 6: Time-dependent normalized discrete total energy (left) and maximum values of the multiscale solution $u_{\text{ms},\ell}$ (right) over time evolution with $\Delta t = 2^{-10}$ in Example 5.2.

where $D = [0, 1]^3$, $T = 0.016$, and $\epsilon = 0.1$. We also consider a highly heterogeneous permeability coefficient κ_3 shown in Figure 4c and the velocity field is $\beta = (y - 0.5, 0.5 - x, 0)^T$, the initial data is $u_0 = 0.1 \sin(\pi x) \sin(\pi y) \sin(\pi z)$.

Multiscale approximation at $T = 0.016$				
H	ϵ_0	CR	ϵ_1	CR
2^{-1}	2.2542E-01	–	3.6893E-01	–
2^{-2}	2.1299E-01	0.0606	3.5376E-01	0.0818
2^{-3}	5.1638E-02	2.0443	1.7974E-01	0.9768
2^{-4}	1.9051E-02	1.4386	7.2222E-02	1.3154

Table 5: Relative errors and convergence rates, for Example 5.3 at $T = 0.016$ with $\ell = 1$ and varying mesh size H .

Numerical results for (5.4) with the fixed level parameter of $\ell = 1$ on each coarse neighborhood with varying coarse grid size are reported in Table 5. Convergence with respect to coarse grid size H and wavelet level ℓ is observed as expected. We notice that the spatial accuracy in the L^2 -norm is just about 1 as expected. Figure 7 depicts the profile of the reference and multiscale solution for problem (5.4) at different instants $t = 0, 0.004, 0.008$ and 0.016 , which visually verifies the accuracy of our multiscale methods.

Example 5.4. In this test, we consider the Schnakenberg reactive model with constant convection, which studies the limit cycle behaviors of two-component chemical reactions

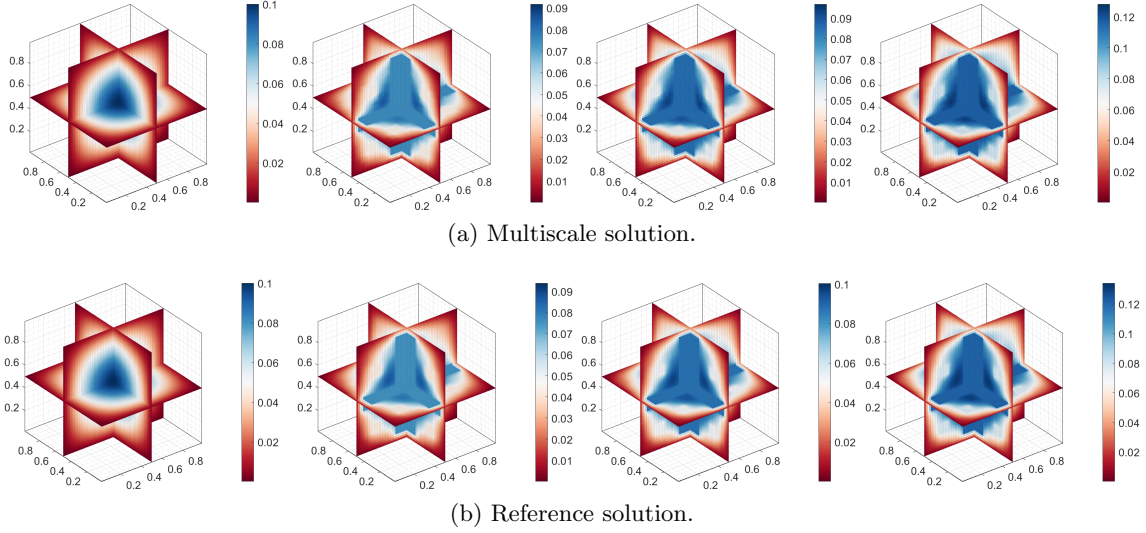


Figure 7: Solutions of Example 5.3 at instants $t = 0, 0.004, 0.008$ and 0.016 (a) Multiscale solution using coarse size of $H = 2^{-4}$ and level parameter $\ell = 2$, and (b) the reference solution.

(Schnakenberg, 1979; Montanelli and Bootland, 2020):

$$\begin{aligned} \partial_t u_1 - \nabla \cdot (\kappa_1 \nabla u_1) + \beta_1 \cdot \nabla u_1 &= \gamma(a - u_1 + u_1^2 u_2), & \text{in } D \times (0, T] \\ \partial_t u_2 - \nabla \cdot (\kappa_2 \nabla u_2) + \beta_2 \cdot \nabla u_2 &= \gamma(b - u_1^2 u_2), & \text{in } D \times (0, T] \end{aligned} \quad (5.5)$$

where u_1 and u_2 represent the concentrations of the chemical species assumed to be maintained at constant concentrations a and b . We take $D := [0, 30] \times [0, 30]$, $T = 5$, $\gamma = 3$, $a = 0.1$ and $b = 0.9$. $\kappa_1 = 1$, $\kappa_2 = 10$ and $\beta_1 = \beta_2 = [-1, -1]^T$ are constant coefficients and constant velocities. The initial data is

$$u_1(x, 0) = 1 - e^{-2[(x-L_x/2.15)^2 + (y-L_x/2.15)^2]}, \quad (5.6)$$

$$u_2(x, 0) = \frac{b}{(a+b)^2} - e^{-2[(x-L_x/2)^2 + (y-L_x/2)^2]}, \quad (5.7)$$

with $L_x = 30$. The simulation is run for 2^9 time steps.

In Table 6, we present the relative errors corresponding to varying coarse mesh size for the problem (5.5) at the final time T . We observe that both relative errors decay as ℓ increases.

Figure 8 depicts the profile of the references and multiscale solutions using our approach to approximate the two-component coupled system (5.5). We can see that the multiscale method can capture most small-scale details of the reference solution.

Multiscale approximation for u_1 at $T = 5$						
H	$\ell = 0$		$\ell = 1$		$\ell = 2$	
	ε_1	ε_0	ε_1	ε_0	ε_1	ε_0
2^{-1}	1.6903E+00	6.3640E-01	1.2440E+00	4.6745E-01	8.8215E-01	3.0306E-01
2^{-2}	6.324E3-01	1.9572E-01	5.4738E-01	1.4371E-01	3.2769E-01	7.0549E-02
2^{-3}	4.0562E-01	9.5299E-02	2.1348E-01	4.0011E-02	1.2758E-01	2.1181E-02
2^{-4}	1.4803E-01	2.0796E-02	4.9016E-02	5.4210E-03	2.0146E-02	3.4661E-03
2^{-5}	3.5231E-02	3.8360E-03	1.2758E-02	3.3414E-03	9.1274E-03	3.3328E-03
Multiscale approximation for u_2 at $T = 5$						
H	$\ell = 0$		$\ell = 1$		$\ell = 2$	
	ε_1	ε_0	ε_1	ε_0	ε_1	ε_0
2^{-1}	7.4820E-01	4.2152E-01	5.3147E-01	2.9112E-01	3.8746E-01	1.6973E-01
2^{-2}	2.6432E-01	1.3413E-01	1.6867E-01	7.5735E-02	7.6502E-02	2.5090E-02
2^{-3}	1.2343E-01	4.7182E-02	5.1759E-02	1.9423E-02	2.4450E-02	9.3365E-03
2^{-4}	2.9775E-02	9.4506E-03	8.8690E-03	1.9526E-03	4.4339E-03	1.5533E-03
2^{-5}	7.8642E-03	1.6049E-03	4.1623E-03	1.5737E-03	3.7082E-03	1.4877E-03

Table 6: Relative errors for Example 5.4 at $T = 5$ with varying parameters (H, ℓ) .

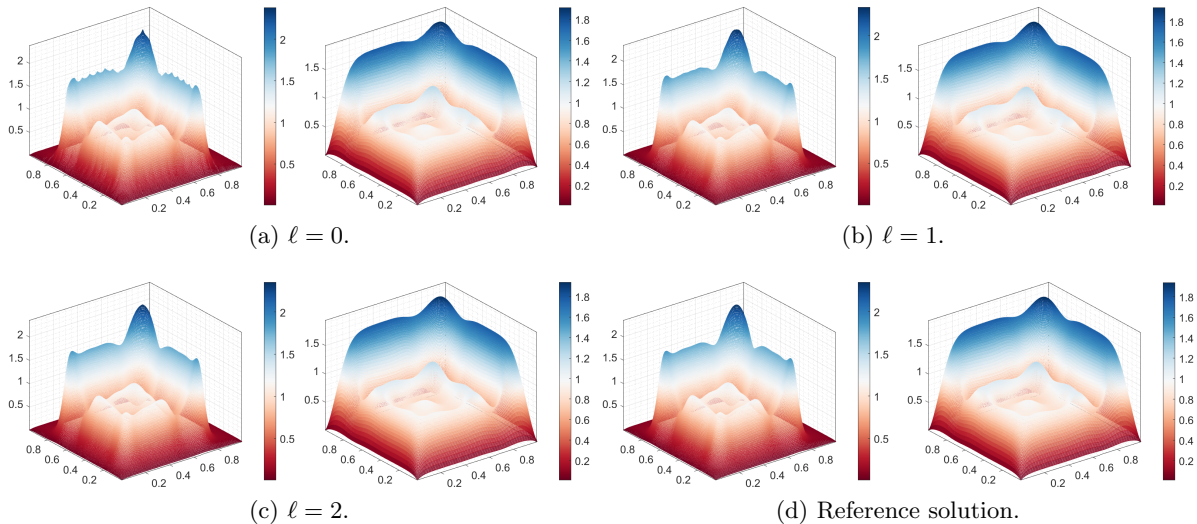


Figure 8: Multiscale solution with 2^9 time-steps with $H = 2^{-4}$ and (a) $\ell = 0$, (b) $\ell = 1$ and (c) $\ell = 2$, and (d) the reference solution of Example 5.4 at final time $T = 5$.

Example 5.5. The last example is to investigate our method for the following Schnakenberg reactive problem with heterogeneous coefficient:

$$\begin{cases} \partial_t u_1 - \nabla \cdot (\kappa_1 \nabla u_1) + \beta_1 \cdot \nabla u_1 &= u_2(1 - u_1), \\ \partial_t u_2 - \nabla \cdot (\kappa_2 \nabla u_2) + \beta_2 \cdot \nabla u_2 &= u_1(1 - u_2^2), \end{cases} \quad (5.8)$$

the permeability coefficients κ_1 and κ_2 are heterogeneous and high-contrast with values of 10^2 in the high-contrast channel constant. Figures 4a–4b plot the permeability fields κ_1 and, κ_2 respectively. Further, for this example. The velocities $\beta_1 = \beta_2$ are given as in the Example 5.2, while the initial conditions are defined as $u_1(x, 0) = \sin(3\pi x) \sin(2\pi y)$ and $u_2(x, 0) = \sin(2\pi x) \cos(3\pi y)$. The terminal time of this simulation is $T = 0.01$, and there are 2^9 time steps. Table 7 lists the relative errors with respect to varying parameters (H, ℓ) at the terminal time T . Similar to Example 5.4, we notice that the errors in levels 1 and 2 decay faster than the first $\ell = 0$ as expected for two solutions in both norms.

Finally, Figure 9 depicts the profile of the reference solutions and multiscale solutions at the terminal time $T = 0.01$. We observe that the multiscale solutions can capture the multiple scales in the reference solutions.

6 Conclusions

We have developed an efficient multiscale method to treat the semilinear parabolic problems with a heterogeneous coefficient. The approximation properties of the corresponding

Multiscale approximation for u_1 at $T = 0.01$						
H	$\ell = 0$		$\ell = 1$		$\ell = 2$	
	ε_1	ε_0	ε_1	ε_0	ε_1	ε_0
2^{-1}	6.3216E-01	5.5896E-01	2.5387E-01	1.4123E-01	1.0218E-01	3.6892E-02
2^{-2}	3.0683E-01	1.8847E-01	1.7760E-01	6.9064E-02	1.3019E-01	4.0238E-02
2^{-3}	2.4723E-01	1.2302E-01	1.2478E-01	3.4178E-02	8.9496E-02	1.7929E-02
2^{-4}	1.8703E-01	7.3334E-02	7.4127E-02	1.1668E-02	4.4538E-02	3.6601E-03
2^{-5}	1.3697E-01	3.8714E-02	4.4229E-02	2.9354E-03	1.9524E-02	5.1187E-03
Multiscale approximation for u_2 at $T = 0.01$						
H	$\ell = 0$		$\ell = 1$		$\ell = 2$	
	ε_1	ε_0	ε_1	ε_0	ε_1	ε_0
2^{-1}	4.3368E-01	2.9545E-01	1.8295E-01	9.2601E-02	9.1993E-02	2.9765E-02
2^{-2}	2.1568E-01	8.3863E-02	1.5276E-01	4.3575E-02	1.3065E-01	4.2853E-02
2^{-3}	1.8089E-01	5.6617E-02	1.0221E-01	1.9836E-02	7.3485E-02	1.0946E-02
2^{-4}	1.2553E-01	2.7039E-02	5.8860E-02	6.0603E-03	3.6188E-02	2.3770E-03
2^{-5}	1.1000E-01	1.8510E-02	3.7821E-02	1.9223E-03	1.5972E-02	2.8104E-03

Table 7: Relative errors for problem (5.8) at the terminal time $T = 0.01$ with varying parameters (H, ℓ) .

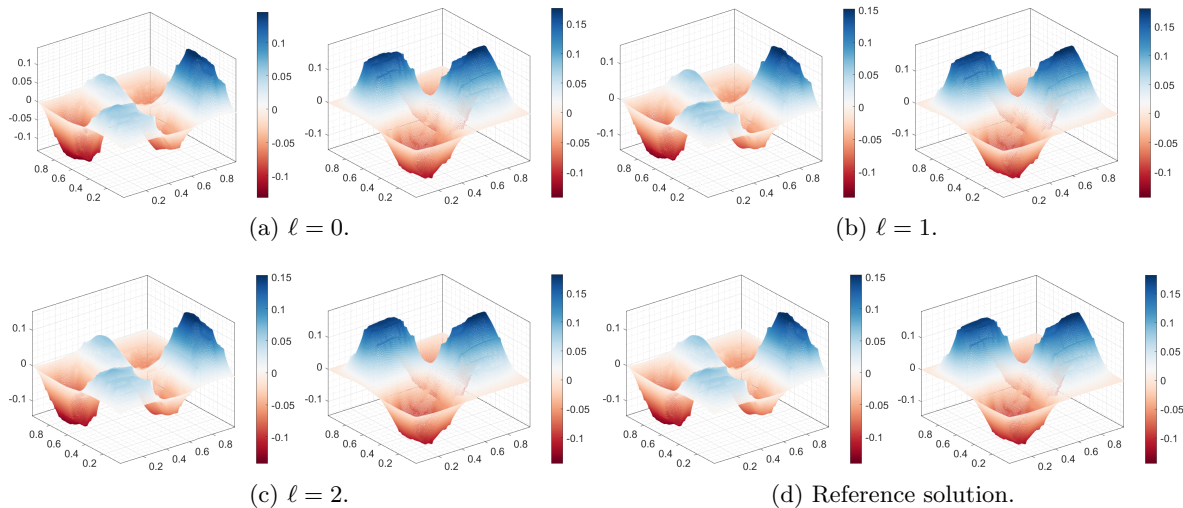


Figure 9: Multiscale solution with 2^9 time-steps using $H = 2^{-4}$ and (a) $\ell = 0$, (b) $\ell = 1$ and (c) $\ell = 2$, and (d) the reference solution of problem (5.8) at final time $T = 0.01$.

steady-state multiscale ansatz space are derived. Since the nonlinear term lies in the reaction term, we can develop a time-independent multiscale ansatz space in this work. The case with the quasilinear term has many important applications, *e.g.*, in the metamaterial, and is more computationally involved and probably requires time-dependent, multiscale ansatz space. We plan to investigate it in the future.

References

Samuel Allen and John Cahn. A microscopic theory for antiphase boundary motion and its application to antiphase domain coarsening. *Acta metallurgica*, 27(6):1085–1095, 1979.

Todd Arbogast, Gergina Pencheva, Mary Wheeler, and Ivan Yotov. A multiscale mortar mixed finite element method. *Multiscale Model. Simul.*, 6(1):319–346, 2007. ISSN 1540-3459. doi: 10.1137/060662587. URL <https://doi.org/10.1137/060662587>.

Sören Bartels. *Numerical methods for nonlinear partial differential equations*, volume 47. Springer, 2015.

Håvard Berland, Bård Skaflestad, and Will M. Wright. Expint—a MATLAB package for exponential integrators. *ACM Trans. Math. Softw.*, 33(1):4–es, mar 2007. ISSN 0098-3500. doi: 10.1145/1206040.1206044. URL <https://doi.org/10.1145/1206040.1206044>.

- Marco Caliari and Fabio Cassini. Efficient simulation of complex Ginzburg–Landau equations using high-order exponential-type methods. *arXiv preprint arXiv:2403.02816*, 2024.
- Marco Caliari, Fabio Cassini, Lukas Einkemmer, and Alexander Ostermann. Accelerating exponential integrators to efficiently solve semilinear advection–diffusion–reaction equations. *SIAM J. Sci. Comput.*, 46(2):A906–A928, 2024. ISSN 1064-8275. doi: 10.1137/23M1562056. URL <https://doi.org/10.1137/23M1562056>.
- Eric Chung, Yalchin Efendiev, and Thomas Y Hou. *Multiscale model reduction–multiscale finite element methods and their generalizations*, volume 212 of *Applied Mathematical Sciences*. Springer, Cham, 2023. ISBN 978-3-031-20408-1; 978-3-031-20409-8. doi: 10.1007/978-3-031-20409-8. URL <https://doi.org/10.1007/978-3-031-20409-8>.
- Philippe G. Ciarlet. *The finite element method for elliptic problems*. North-Holland Publishing Co., Amsterdam-New York-Oxford, 1978. ISBN 0-444-85028-7.
- Luis Contreras, David Pardo, Eduardo. Abreu, Judith Muñoz Matute, Ciro Diaz, and Juan Galvis. An exponential integration generalized multiscale finite element method for parabolic problems. *J. Comput. Phys.*, 479:Paper No. 112014, 14, 2023. ISSN 0021-9991. doi: 10.1016/j.jcp.2023.112014. URL <https://doi.org/10.1016/j.jcp.2023.112014>.
- Weinan E and Bjorn Engquist. The heterogeneous multiscale methods. *Commun. Math. Sci.*, 1(1):87–132, 2003. ISSN 1539-6746. URL <http://projecteuclid.org/euclid.cms/1118150402>.
- Yalchin Efendiev, Juan Galvis, and Thomas Y Hou. Generalized multiscale finite element methods (GMsFEM). *J. Comput. Phys.*, 251:116–135, 2013. ISSN 0021-9991. doi: 10.1016/j.jcp.2013.04.045. URL <https://doi.org/10.1016/j.jcp.2013.04.045>.
- Shubin Fu, Eric Chung, and Guanglian Li. Edge multiscale methods for elliptic problems with heterogeneous coefficients. *J. Comput. Phys.*, 396:228–242, 2019. ISSN 0021-9991. doi: 10.1016/j.jcp.2019.06.006. URL <https://doi.org/10.1016/j.jcp.2019.06.006>.
- Shubin Fu, Guanglian Li, Richard Craster, and Sebastien Guenneau. Wavelet-based edge multiscale finite element method for Helmholtz problems in perforated domains. *Multiscale Model. Simul.*, 19(4):1684–1709, 2021. ISSN 1540-3459. doi: 10.1137/19M1267180. URL <https://doi.org/10.1137/19M1267180>.
- Shubin Fu, Eric Chung, and Guanglian Li. Wavelet-based edge multiscale finite element methods for singularly perturbed convection–diffusion equations. *arXiv preprint arXiv:2309.12108*, 2023.
- Daniel Henry. *Geometric theory of semilinear parabolic equations*, volume 840 of *Lecture Notes in Mathematics*. Springer-Verlag, Berlin-New York, 1981. ISBN 3-540-10557-3.

- Marlis Hochbruck and Alexander Ostermann. Explicit exponential Runge–Kutta methods for semilinear parabolic problems. *SIAM J. Numer. Anal.*, 43(3):1069–1090, 2005. ISSN 0036-1429. doi: 10.1137/040611434. URL <https://doi.org/10.1137/040611434>.
- Marlis Hochbruck and Alexander Ostermann. Exponential integrators. *Acta Numerica*, 19: 209–286, 2010.
- Marlis Hochbruck, Christian Lubich, and Hubert Selhofer. Exponential integrators for large systems of differential equations. *SIAM J. Sci. Comput.*, 19(5):1552–1574, 1998. ISSN 1064-8275. doi: 10.1137/S1064827595295337. URL <https://doi.org/10.1137/S1064827595295337>.
- Thomas Y Hou and Xiao-Hui Wu. A multiscale finite element method for elliptic problems in composite materials and porous media. *J. Comput. Phys.*, 134(1):169–189, 1997. ISSN 0021-9991.
- Thomas J R Hughes, Gonzalo R Feijóo, Luca Mazzei, and Jean-Baptiste Quinicy. The variational multiscale method—a paradigm for computational mechanics. *Comput. Methods Appl. Mech. Engrg.*, 166(1-2):3–24, 1998. ISSN 0045-7825. doi: 10.1016/S0045-7825(98)00079-6. URL [https://doi.org/10.1016/S0045-7825\(98\)00079-6](https://doi.org/10.1016/S0045-7825(98)00079-6).
- Stig Larsson. Nonsmooth data error estimates with applications to the study of the long-time behavior of finite element solutions of semilinear parabolic problems. *preprint 1992-36, Department of Mathematics, Chalmers University of Technology*, 1992.
- Guanglian Li. On the convergence rates of GMsFEMs for heterogeneous elliptic problems without oversampling techniques. *Multiscale Model. Simul.*, 17(2):593–619, 2019. ISSN 1540-3459. doi: 10.1137/18M1172715. URL <https://doi.org/10.1137/18M1172715>.
- Guanglian Li. Wavelet-based edge multiscale parareal algorithm for subdiffusion equations with heterogeneous coefficients in a large time domain. *J. Comput. Appl. Math.*, 440: Paper No. 115608, 24, 2024. ISSN 0377-0427. doi: 10.1016/j.cam.2023.115608. URL <https://doi.org/10.1016/j.cam.2023.115608>.
- Guanglian Li and Jiuhua Hu. Wavelet-based edge multiscale parareal algorithm for parabolic equations with heterogeneous coefficients and rough initial data. *J. Comput. Phys.*, 444:Paper No. 110572, 18, 2021. ISSN 0021-9991. doi: 10.1016/j.jcp.2021.110572. URL <https://doi.org/10.1016/j.jcp.2021.110572>.
- Jacques Louis Lions and Enrico Magenes. *Non-homogeneous boundary value problems and applications*, volume I. Springer-Verlag, New York-Heidelberg, 1972.
- Axel Målqvist and Daniel Peterseim. Localization of elliptic multiscale problems. *Math. Comp.*, 83(290):2583–2603, 2014. ISSN 0025-5718.

doi: 10.1090/S0025-5718-2014-02868-8. URL <https://doi.org/10.1090/S0025-5718-2014-02868-8>.

Jens Melenk and Ivo Babuška. The partition of unity finite element method: basic theory and applications. *Comput. Methods Appl. Mech. Engrg.*, 139(1-4):289–314, 1996. ISSN 0045-7825. doi: 10.1016/S0045-7825(96)01087-0. URL [https://doi.org/10.1016/S0045-7825\(96\)01087-0](https://doi.org/10.1016/S0045-7825(96)01087-0).

Hadrien Montanelli and Niall Bootland. Solving periodic semilinear stiff PDEs in 1D, 2D and 3D with exponential integrators. *Math. Comput. Simulation*, 178:307–327, 2020. ISSN 0378-4754. doi: 10.1016/j.matcom.2020.06.008. URL <https://doi.org/10.1016/j.matcom.2020.06.008>.

Bagus Putra Muljadi, Jacek Narski, Alexei Lozinski, and Pierre Degond. Nonconforming multiscale finite element method for Stokes flows in heterogeneous media. Part I: Methodologies and numerical experiments. *Multiscale Model. Simul.*, 13(4):1146–1172, 2015. ISSN 1540-3459. doi: 10.1137/14096428X. URL <https://doi.org/10.1137/14096428X>.

Leonardo A Poveda, Juan Galvis, and Eric Chung. A second-order exponential integration constraint energy minimizing generalized multiscale method for parabolic problems. *J. Comput. Phys.*, 502:Paper No. 112796, 2024. ISSN 0021-9991. doi: 10.1016/j.jcp.2024.112796. URL <https://doi.org/10.1016/j.jcp.2024.112796>.

Jürgen Schnakenberg. Simple chemical reaction systems with limit cycle behaviour. *Journal of Theoretical Biology*, 81(3):389–400, 1979. ISSN 0022-5193. doi: [https://doi.org/10.1016/0022-5193\(79\)90042-0](https://doi.org/10.1016/0022-5193(79)90042-0). URL <https://www.sciencedirect.com/science/article/pii/0022519379900420>.

Antoine Tambue. An exponential integrator for finite volume discretization of a reaction–advection–diffusion equation. *Comput. Math. Appl.*, 71(9):1875–1897, 2016. ISSN 0898-1221. doi: 10.1016/j.camwa.2016.03.001. URL <https://doi.org/10.1016/j.camwa.2016.03.001>.

Vidar Thomée. *Galerkin finite element methods for parabolic problems*, volume 25 of *Springer Series in Computational Mathematics*. Springer-Verlag, Berlin, second edition, 2006. ISBN 978-3-540-33121-6; 3-540-33121-2.